

April 5 1993
UTHEP-256

Charged fermion states in the quenched U(1) chiral Wilson-Yukawa model

S. Aoki, H. Hirose and Y. Kikukawa

Institute of Physics, University of Tsukuba,
Tsukuba, Ibaraki-305, Japan

Abstract

Property of charged fermion states is investigated in the quenched U(1) chiral Wilson-Yukawa model. Fitting the charged fermion propagator with a single hyperbolic cosine does not yield reliable results. On the other hand the behavior of the propagator including large lattice size dependence is well described by the large Wilson-Yukawa coupling expansion, providing strong evidence that no charged fermion state exists as an asymptotic particle in this model.

1 Introduction

The effort toward construction of chiral gauge theories on the lattice is primarily motivated by the fact that a full nonperturbative understanding of the standard $SU(2) \times U(1)_Y$ electroweak theory is required to answer a variety of unsolved questions such as the upper bound of the Higgs boson and fermion masses in the full theory and the magnitude of the baryon number violation in the standard model. The lattice approach provides a potentially useful tool for these purposes. However, there is a serious difficulty in this approach: because of fermion doubling[1, 2], each lattice fermion field yields 16 fermion modes, half of which has one chirality and the other half the opposite chirality, so that the lattice theory is non-chiral. There are several attempts to avoid this difficulty. Among the proposals, the Wilson-Yukawa formulation [3, 4, 5, 6] has been extensively investigated during the last few years. In particular it has been found through numerical studies[7, 8, 9] and analytical work[10, 11, 12, 13] that the fermion doublers decouple in the continuum limit if the Wilson-Yukawa coupling is sufficiently large.

Recently it has been reported[14] in a quenched simulation of a $U(1)$ chiral model that the charged fermion mass is approximately equal to the sum of the neutral fermion mass and the scalar boson mass on a $12^3 \times 16$ lattice. This relation suggests that the charged state is a scattering state of the neutral fermion and the scalar boson, and is not a bound state. Based on this interpretation it was claimed that charged fermion states do not exist in the symmetric phase of the global chiral model for strong Wilson-Yukawa coupling, and hence the Wilson-Yukawa formulation fails.

It should be noted, however, that a large finite size effect is seen in the data of ref.[14] for charged fermion propagators between $8^3 \times 16$ and $12^3 \times 16$ lattices and that the relation among the masses does not hold on an $8^3 \times 16$ lattice. Thus much further analysis of the model, especially a systematic study of finite size effect, is needed to see if the conclusion is tenable. We have carried out such an analysis and we report on the results in this article.

The organization of this article is as follows. In Sect.2, we define the action of the $U(1)$ chiral model we study and consider several bosonic and fermionic field operators, especially the two kinds of Dirac fermions, neutral and charged. We measure two-point correlation functions of these operators in the simulation whose parameters are also summarized. In Sect.3 spectra in the broken phase are investigated. We extract masses of neutral and charged

fermions as well as those of scalar particles. In Sect.4 we present and discuss the results of our Monte Carlo simulation in the symmetric phase in detail. Emphasis is placed on the fermionic charged state, which has been argued not to exist as a single particle in this phase[14]. Finite size effects for the charged fermion state are examined by means of the large Wilson-Yukawa coupling expansion. Our conclusions are summarized in Sect.5.

2 U(1) chiral model

2.1 The action

We investigate a chiral U(1) Higgs-fermion system in the Wilson-Yukawa formulation with the action given by

$$\begin{aligned} S_{total} &= S_{boson} + S_{free} + S_{yukawa} + S_{wilson-yukawa} \\ &\equiv S_{boson} + S_{fermion}, \end{aligned} \quad (1)$$

$$S_{boson} = -2\kappa \sum_{n,\mu} \text{Re}(g_n^\dagger g_{n+\mu}), \quad (2)$$

$$S_{free} = -\frac{1}{2} \sum_{n,\mu} (\bar{\psi}_n \gamma_\mu \psi_{n+\mu} - \bar{\psi}_{n+\mu} \gamma_\mu \psi_n), \quad (3)$$

$$S_{yukawa} = y \sum_n \bar{\psi}_n (g_n^\dagger P_L + g_n P_R) \psi_n, \quad (4)$$

$$\begin{aligned} S_{wilson-yukawa} &= -\frac{w}{2} \sum_{n,\mu} \bar{\psi}_n P_L (g_{n+\mu}^\dagger \psi_{n+\mu} + g_{n-\mu}^\dagger \psi_{n-\mu} - 2g_n^\dagger \psi_n) \\ &\quad -\frac{w}{2} \sum_{n,\mu} \bar{\psi}_n P_R g_n (\psi_{n+\mu} + \psi_{n-\mu} - 2\psi_n). \end{aligned} \quad (5)$$

Here g_n is a non-linear U(1) scalar field satisfying $g_n^\dagger g_n = 1$, and κ, y and w are the hopping parameter of the boson, the Yukawa coupling constant, and the Wilson-Yukawa coupling constant respectively. The phase transition between the broken phase and the symmetric phase occurs at $\kappa_c = 0.149$ in the quenched theory. The action S_{total} is invariant under a global $U(1)_L \times U(1)_R$ transformation given by

$$\begin{aligned} g_n &\rightarrow \Omega_L g_n \Omega_R^\dagger, & \Omega_{L,R} &\in U(1)_{L,R}, \\ \psi_n &\rightarrow (\Omega_L P_L + \Omega_R P_R) \psi_n, \\ \bar{\psi}_n &\rightarrow \bar{\psi}_n (\Omega_L^\dagger P_R + \Omega_R^\dagger P_L). \end{aligned}$$

The scalar field g and the *chiral* fermion fields ψ_L and ψ_R are assigned the charges $(Q_L, Q_R) = (1, -1)$, $(1, 0)$ and $(0, 1)$, respectively.

We consider two kinds of *Dirac* fermion fields in our study defined by

$$N_n = (g_n^\dagger P_L + P_R)\psi_n, \quad \bar{N}_n = \bar{\psi}_n(g_n P_L + P_R), \quad (6)$$

with the charge (0,1) and

$$C_n = (P_L + g_n P_R)\psi_n, \quad \bar{C}_n = \bar{\psi}_n(P_L + g_n^\dagger P_R) \quad (7)$$

with the charge (1,0). The fermion fields N_n and C_n are usually called “neutral” and “charged” in view of the eventual gauging of the global $U(1)_L$ symmetry. This distinction is not important since N_n will be the “charged” fermion if the $U(1)_R$ symmetry is gauged. The most important distinction between N_n and C_n is that the Wilson-Yukawa coupling is reduced to an ordinary Wilson term and the Yukawa coupling to a mass term for the neutral fermion N_n . In fact one easily sees that

$$\begin{aligned} S_{fermion} = & -\frac{1}{2} \sum_{n,\mu} \bar{N}_n \gamma_\mu P_L g_n^\dagger (g_{n+\mu} N_{n+\mu} - g_{n-\mu} N_{n-\mu}) \\ & -\frac{1}{2} \sum_{n,\mu} \bar{N}_n \gamma_\mu P_R (N_{n+\mu} - N_{n-\mu}) \\ & + y \sum_n \bar{N}_n N_n \\ & -\frac{w}{2} \sum_{n,\mu} \bar{N}_n (N_{n+\mu} + N_{n-\mu} - 2N_n). \end{aligned} \quad (8)$$

Furthermore, the right-handed component of the neutral fermion has the shift symmetry[16]. Consequently, it is expected to appear as a massless particle at the point $y = 0$. It has been shown ([7]–[13]) that the physical fermion state of the N_n field appears in the continuum limit while doublers of the N_n are decoupled when the Wilson-Yukawa coupling w is large enough ($w \sim O(1)$).

In terms of the charged fermion, on the other hand, the action is written as

$$S_{fermion} = -\frac{1}{2} \sum_{n,\mu} \bar{C}_n \gamma_\mu P_L (C_{n+\mu} - C_{n-\mu})$$

$$\begin{aligned}
& -\frac{1}{2} \sum_{n,\mu} \bar{C}_n \gamma_\mu P_R g_n (g_{n+\mu}^\dagger C_{n+\mu} - g_{n-\mu}^\dagger C_{n-\mu}) \\
& + y \sum_n \bar{C}_n C_n \\
& - \frac{w}{2} \sum_{n,\mu} \bar{C}_n g_n (g_{n+\mu}^\dagger C_{n+\mu} + g_{n-\mu}^\dagger C_{n-\mu} - 2g_n^\dagger C_n).
\end{aligned} \tag{9}$$

Since $w \sim O(1)$ is needed for the doublers to decouple, the field C_n interacts strongly with the scalar field through the Wilson-Yukawa coupling. We investigate this strongly coupled system through the Monte Carlo simulation.

2.2 Observables

In order to extract the properties of the scalar state of the model, we consider three different correlation functions at zero spatial momentum defined by

$$\begin{aligned}
D_\sigma(t) &= \sum_{\vec{n}} \langle \sigma_{(\vec{0},0)} \sigma_{(\vec{n},t)} \rangle_c, \\
D_\pi(t) &= \sum_{\vec{n}} \langle \pi_{(\vec{0},0)} \pi_{(\vec{n},t)} \rangle_c, \\
D_g(t) &= \sum_{\vec{n}} \langle g_{(\vec{0},0)}^\dagger g_{(\vec{n},t)} \rangle_c,
\end{aligned} \tag{10}$$

where $\sigma_n = \text{Re}(g_n)$, $\pi_n = \text{Im}(g_n)$ and $\langle \quad \rangle_c$ means the connected part of correlation functions.

In the symmetric phase (at $\kappa < \kappa_c = 0.149$ in the quenched approximation), only one massive scalar state is expected. Hence making a fit of form

$$D_\phi(t) = A_\phi \cosh[E_\phi(t - T/2)] \tag{11}$$

with T the temporal lattice size should yield consistent values for the energy E_ϕ independent of the choice $\phi = g, \sigma, \pi$.

The parameters A_ϕ and E_ϕ are related to the wave function renormalization constant Z_ϕ and the mass parameter m_ϕ in the momentum-space-propagator through

$$\begin{aligned}
Z_\phi &= 2A_\phi \sinh(E_\phi) \sinh(E_\phi T/2), \\
m_\phi^2 &= 2 \cosh(E_\phi) - 2.
\end{aligned} \tag{12}$$

In the broken phase (at $\kappa < \kappa_c$), the scalar field develops a vacuum expectation value and the symmetry $U(1)_L \times U(1)_R$ is broken down to $U(1)_{L=R}$. For a finite volume, however, fluctuation of the Nambu-Goldstone mode makes the expectation value of the scalar field vanish in absence of an external field. To avoid this problem, each scalar field configuration is rotated globally so that it satisfies $\sum_n \pi_n = 0$. Consequently $v \equiv \langle g \rangle = \langle \sigma \rangle$ and the massive σ propagator can be fitted by the same form as before. The form of the propagator for the Nambu-Goldstone boson is determined by the chiral perturbation theory[17] which gives

$$D_\pi(t) = A + B \left(\left(\frac{t}{T} - \frac{1}{2} \right)^2 - \frac{1}{12} \right), \quad (13)$$

where $Z_\pi = 4B/T$. From the constraint $\sum_t D_\pi(t) = 0$ A and B are related by $A = -B/6T^2$. In our fit we take A and B as free parameters and check this relation for fitted results.

For the neutral fermion, a general expression for the propagator follows from the shift symmetry[16]:

$$S_F^{-1}(p) = i \sum_\mu \gamma_\mu \sin(p_\mu) (\mathcal{A}_\mu^L(p) P_L + \mathcal{A}_\mu^R(p) P_R) + \mathcal{B}(p), \quad (14)$$

$$\mathcal{A}_\mu^R(p) = 1 \equiv 1/Z^R, \quad (15)$$

$$\mathcal{B}(p) = y + w \sum_\mu (1 - \cos(p_\mu)). \quad (16)$$

The form of the function $\mathcal{A}_\mu^L(p)$ can be evaluated with several analytical methods[11, 12, 13]. The results are identical in the leading order, giving

$$\mathcal{A}_\mu^L(p) = \langle g_{n+\mu}^\dagger g_n \rangle = z^2 \equiv 1/Z^L. \quad (17)$$

In this approximation, the propagator at the zero spatial momentum takes the form

$$\sum_{\vec{n}} \langle N_{(\vec{0},0)} \bar{N}_{(\vec{n},t)} \rangle = P_L \gamma_0 S_N^L(t) + P_R \gamma_0 S_N^R(t) + S_N^M(t).$$

where

$$S_N^{L,R}(t) = A_N^{L,R} \left(\frac{\cosh(E_N^-(t - T/2))}{\cosh(E_N^- T/2)} - \frac{\cosh(E_N^+(t - T/2))}{\cosh(E_N^+ T/2)} \right),$$

$$S_N^M(t) = A_N^M \left(\frac{\sinh(E_N^-(t - T/2))}{\cosh(E_N^-T/2)} \cdot \frac{m + r(1 - \cosh E_N^-)}{\sinh E_N^-} - \frac{\sinh(E_N^+(t - T/2))}{\cosh(E_N^+T/2)} \cdot \frac{m + r(1 - \cosh E_N^+)}{\sinh E^+ - N} \right) \quad (18)$$

with

$$m = y\sqrt{Z^L Z^R}, \quad r = w\sqrt{Z^L Z^R}, \quad (19)$$

$$A_N^{L,R} = \frac{Z^{L,R}}{2(m^2 + 2rm + 1)^{1/2}}, \quad (20)$$

$$A_N^M = \frac{\sqrt{Z^L Z^R}}{2(m^2 + 2rm + 1)^{1/2}}, \quad (21)$$

$$\exp(E_N^\pm) = \frac{m + r + \sqrt{m^2 + 2rm + 1}}{r \mp 1}. \quad (22)$$

Here E_N^- (E_N^+) is the mass of the physical fermion (the time doubler). With the replacement $y \rightarrow y + 2w$, the formula (18) applies to the (spatial) doubler mode at $\vec{p} = (\pi, 0, 0)$. We denote its mass as E_{ND} .

We use the form (18) taking E_N^\pm and $A_N^{L,R,M}$ as free parameters in order to fit S_N^L , S_N^R and S_N^M separately. The doubler propagator is fitted with the first term in (18) because its “time doubler” is much heavier. We will also compare data to the semi-analytical prediction (18) with the Monte Carlo estimation of z^2 as an input.

For the charged fermion, the form of the propagator is not known. We found that the formula (18) does not fit the charged fermion propagator well. We therefore tried a single pole form[14] for the fit given by

$$S_C^{L,R}(t) = A_C^{L,R} \cosh(E_C(t - T/2)). \quad (23)$$

We extract the mass E_C using the data over a time interval $t_{min} \leq t \leq T - t_{min}$, varying t_{min} in order to see whether the mass is stable.

2.3 Simulation

Our simulation is performed in the quenched approximation on $8^3 \times 16$ and $12^3 \times 16$ lattices. Scalar field configurations are generated by the 10 hit

Metropolis algorithm and the cluster algorithm of ref.[18] at $\kappa = 0.16$ (broken phase) and at $\kappa = 0.145$ (symmetric phase). See Table 1 for statistics.

The fermion propagators are calculated by the conjugate gradient method with the point-source in the broken phase and the wall-source in the symmetric phase. The anti-periodic (periodic) boundary condition in the time direction (the spatial directions) is used. We fix the Wilson-Yukawa coupling at $w = 1$ and vary the Yukawa coupling y . The statistics depends on the simulation parameters. Typically, 2,400 (400) configurations separated by 500 (200) sweeps are accumulated at $\kappa = 0.145(0.16)$ for the charged fermion propagator on an $8^3 \times 16$ lattice. See Table 2 for further details.

Errors are all estimated with the jack-knife method, using the bin size as listed in Table 1 and Table 2. For example, for bosonic observables on an $8^3 \times 16$ lattice at $\kappa = 0.16$, each bin consists of the average of successive 20,000 (10,000) sweeps and the number of the bins is 4 (8) with the Metropolis (cluster) algorithm.

3 Results for the broken phase

The π propagator in the broken phase is shown in Fig.1 together with the fit of form (13) expected from the chiral perturbation theory. Fit is excellent with $A = -0.0218(52)$ and $B = 23.7(2)$, which satisfies the constraint $A = -B/6T^2 = -0.0154(1)$ within 1.3σ .

The σ propagator is shown in Fig.2 together with the fit of form (11). The data points around $t = T/2$ lie above the fitting curve. We observed a similar behavior for the scalar field propagator obtained with the cluster algorithm[18]. This behavior may be related to the rotation procedure for calculating $D_\sigma(t)$ in the broken phase.

The masses and the wave function renormalization constants Z_ϕ as well as the values of v and z^2 are listed in Table 3. From the results we estimate the renormalized self coupling constant:

$$\lambda_R = 3\left(\frac{am_\sigma}{av}\right)^2 Z_\sigma = 32.4(2). \quad (24)$$

The tree-level unitarity bound for the $O(n)$ scalar model is $\lambda_R < 48\pi(n+1)^{-1} = 50.2(n=2)[19]$.

In the broken phase we expect the relation $E_N = E_C$ between the energy of the charged and the neutral fermion since they have the same quantum number under the residual $U(1)_{L+R}$ symmetry. This also can be seen from the following equation

$$\langle C_0 \bar{C}_n \rangle = v^2 \langle N_0 \bar{N}_n \rangle + \dots$$

We fit the neutral fermion propagator with (18) and the charged fermion propagator with (23). Our results for E_N and E_C are plotted in Fig.3 by open circles and squares. (see Table 4 for numerical values.) They agree perfectly and also with the analytic prediction of the hopping parameter expansion[12, 13, 15] drawn by dotted lines. Thus our results in the broken phase confirm the relation $E_N = E_C$ assumed in refs.[7, 9]. (The relation $E_N \simeq E_C$ in the broken phase has been also observed in ref.[8] using the momentum space propagators.) It is also seen in Fig.3 that the mass of the neutral fermion doubler E_{ND} (solid circles) remains $O(1)$ in the $y \rightarrow 0$ limit.

4 Spectrum in the symmetric phase

4.1 Scalar field

The simulation has been performed with the parameters summarized in Table 1. The scalar propagator $D_g(t)$ is shown in Fig.4 together with the fit. It is seen that finite-size effects are small. The result for the mass of the scalar field is summarized in Table 3. We have checked that these values are insensitive to the fitting range. Our value $E_g = 0.415(1)$ on an $8^3 \times 16$ lattice obtained with the Metropolis algorithm is substantially larger than the value¹ $E_g = 0.387(9)$ of ref.[14], which employed the cluster algorithm[18]. In order to make a direct comparison we generated 120,000 configurations with the same cluster algorithm and found $E_g = 0.413(3)$ on an $8^3 \times 16$ lattice, which perfectly agrees with our Metropolis value quoted above. Thus the discrepancy is not caused by a different choice of the algorithm. For those who may be interested in resolving this problem, we provide our data of $D_g(t)$ in Table 5.

4.2 Neutral fermion

The calculation of the neutral fermion propagator has been performed with the parameters in Table 2. The propagator data on an $8^3 \times 16$ lattice are shown in Fig.5. The propagators calculated through (18)(dotted curves in Fig.5) agree with the data. Fitted values of the energy E_N^\pm are given in Table 6 and are plotted as a function of y in Fig.6 together with the prediction of the hopping parameter expansion. Again it is seen that the hopping parameter expansion agrees with the data. Finite size effects for E_N are very small.

4.3 Charged fermion

The propagator of the charged fermion S_C^L is shown in Fig.7. We observe a large finite size effect between $8^3 \times 16$ and $12^3 \times 16$ lattices. As mentioned before we found that the propagators can not be fitted by the free fermion ansatz. We have therefore tried to extract the mass through a fit of the form (23) over the range $t_{min} \leq t \leq T - t_{min}$. The value of E_C as a function of t_{min} is plotted in Fig.8. Since the value of E_C significantly changes with

¹This is calculated from the value $m_g = 0.390(9)$ quoted in ref.[15] using(12)

the variation of t_{min} , the charged fermion mass can not be extracted reliably by the fit. We are therefore not able to confirm the relation claimed in ref.[14] that $E_C \simeq E_N + E_g$ on a $12^3 \times 16$ lattice. We should comment that our propagator numerically differs from that of ref.[14] by 3 to 5 standard deviations, exhibiting a faster decrease with t . (See Fig.7.) Our data of S_C^L for both sizes are given in Table 5. The discrepancy probably originates from the difference of the scalar field configurations noted before.

4.4 Interpretation of charged fermion state

In order to understand the nature of the charged fermion state, we have to find a good explanation for both the t dependence of the rest energy E_c and the large finite size effect of the propagator.

It has been reported in ref.[15] that the large Wilson-Yukawa coupling expansion explains the data of ref.[14]. However, the agreement is only qualitative. In addition our charged fermion propagator is different from that of ref.[14] and their results for the scalar mass and the wave function renormalization constant, which were used in the calculation of ref.[15] as an input, are also different from ours. Furthermore the large finite size effect of the charged fermion propagator was not discussed in terms of the large Wilson-Yukawa coupling expansion in ref.[15]. We therefore think that a reanalysis of our data in terms of the large Wilson-Yukawa coupling expansion is necessary.

We have performed the expansion for the charged fermion propagator up to the next-to-leading order as in ref.[15]. To this order the analytic expression for $S_C^L(t)$ is given by

$$S_C^L(t) = \frac{\alpha^2}{4} S_{conv.}^L(t) - \frac{1}{2} \left(\frac{\alpha}{4} \right)^4 \left(\sum_{t_1} S_{conv.}^L(t - t_1) (\nabla_{t_1} S_{conv.}^L(t_1)) + W_L^{(4)}(t) \right), \quad (25)$$

where $\alpha = 4/(4w + y)$ is the expansion parameter and $\nabla_t f(t) = f(t + 1) - f(t - 1)$. The leading order contribution

$$S_{conv.}^L(t) = \frac{1}{L^3} \sum_{\vec{k}} S_N^L(t, \vec{k}) D_g(t, -\vec{k})$$

is the convolution of the neutral fermion propagator

$$S_N^L(t, \vec{k}) = \frac{1}{T} \sum_{k_0} e^{ik_0 t} \frac{-i \sin(k_0)}{(\alpha z/4)^2 \sum_{\lambda} \sin^2(k_{\lambda}) + (1 - \alpha w/4 \sum_{\lambda} \cos(k_{\lambda}))^2}$$

and the scalar propagator

$$D_g(t, \vec{p}) = \frac{1}{T} \sum_{p_0} e^{ip_0 t} \frac{Z_g}{2 \sum_{\lambda} (1 - \cos(p_{\lambda})) + m_g^2}.$$

The boundary conditions in the time direction imply $k_0 T = (2n+1)\pi$ for the fermion field and $p_0 T = 2n\pi$ for the scalar field, where $n = 0, 1, \dots, T-1$. In (25), $W_L^{(4)}(t)$ is the left-handed part of the 4-point-vertex contribution given by

$$\begin{aligned} W^{(4)}(n_0) &= \sum_{\vec{n}} \sum_{\xi, \mu} (S_N(n - \xi) \gamma_{\mu} S_N(\xi + \hat{\mu}) - S_N(n - \xi - \hat{\mu}) \gamma_{\mu} S_N(\xi)) \\ &\quad \times G^{(4)}(n, \xi, \xi + \hat{\mu}), \end{aligned}$$

with

$$S_N(n) = (P_R + P_L \frac{4}{\alpha}) < N_{(\vec{0}, 0)} N_{(\vec{n}, n_0)} > (P_L + P_R \frac{4}{\alpha}),$$

where $G^{(4)}$ is the bosonic 4-point Green's function. Following ref.[15] we take the mean-field result for $G^{(4)}$. Similar formulae can be obtained for S_C^R and S_C^M . See ref.[15] for details.

In order to compute the right handed side of (25) we use the values of Z_g , m_g and z^2 determined in our numerical simulation results for S_C^L and the simulation data for the two lattices are compared in Fig.9 for $y = 0.4$ and in Fig.10 for $y = 0.1$. The agreement between the data and the prediction is excellent at $y = 0.4$ and is very good even at $y = 0.1$.

The leading order contribution to S_C^L is the convolution of the neutral fermion propagator and the scalar propagator, each of which has very small lattice size dependence. It turns out, however, that their convolution has a large size dependence, which explains the size effect in our data. The next-to-leading order correction is found to be relatively small. The analytic predictions for S_C^R and S_C^M also agree with the data very well. (See Fig.11 and Fig.12).

As a further check, we have performed the large Wilson-Yukawa coupling expansion of the charged fermion propagator in the broken phase. In this case the disconnected part has to be separated out from the two-point function of the scalar field, and the connected part is the sum of contributions from the massless Nambu-Goldstone boson and the massive real scalar particle. Therefore, we should add the following contribution

$$v^2 \sum_{\vec{k}} S_N^L(t, \vec{k})$$

to (25) and replace the scalar propagator $D_g(t, \vec{p})$ with the sum of those for the Nambu-Goldstone boson and for the real scalar particle:

$$\frac{1}{T} \sum'_{p_0} e^{ip_0 t} \frac{Z_\pi}{2 \sum_\lambda (1 - \cos(p_\lambda))} + \frac{1}{T} \sum_{p_0} e^{ip_0 t} \frac{Z_\sigma}{2 \sum_\lambda (1 - \cos(p_\lambda)) + m_\sigma^2}.$$

Here \sum' means that $p_0 = 0$ is omitted in the sum for $\vec{p} = 0$. The results up to the next-to-leading order are plotted in Fig.13. The expansion works well also in the broken phase.

Within the large Wilson-Yukawa coupling expansion it has been shown in ref.[15] that the charged fermion is a scattering state of the scalar particle and the neutral fermion. The good agreement between the data and the result of the expansion therefore provides strong evidence that no charged fermion exists as a single particle state in the symmetric phase.

5 Conclusion

We have investigated the spectrum of fermions in the Wilson-Yukawa formulation through a quenched simulation of the U(1) chiral Wilson-Yukawa model. In the broken phase the neutral fermion state exists and the charged fermion operator generates the same state. In the symmetric phase the charged fermion mass can not be extracted by a single hyperbolic cosine fit even at large t and charged fermion propagators suffer a large finite size effect. We found that not only this large finite size effect but also the form of charged fermion propagators can be explained by the large Wilson-Yukawa coupling expansion. Within the expansion the charged fermion in the symmetric phase is interpreted as a scattering state of the scalar boson and the

neutral fermion. We conclude that no charged fermion exists as a single particle asymptotic state in the Wilson-Yukawa model in *both* phases. Only the scalar boson and the “neutral” Dirac fermion exist in this model. Although our data differ from those of ref.[14] and our reasoning which leads to our conclusion is quite different, we agree on the nature of the charged fermion state in the Wilson-Yukawa formulation.

We can generalize this conclusion as follows. In more complicated chiral models with the Wilson-Yukawa coupling, we can always redefine fermionic field variables so that the Wilson-Yukawa coupling turns into a free Wilson mass term. Only those states generated by such field variables can appear as fermionic single particle states in the strong Wilson-Yukawa coupling region. And these states are necessarily Dirac fermions with vector-like global charges. Their interaction with the scalar fields are weak in general.

Acknowledgments

Numerical calculations for the present work were carried out on HITAC S820/80 at KEK. We thank the Theory Division of KEK for warm hospitality. The data analysis program SALS[20] was used for fittings in this article. We also thank Prof. Kanaya and Prof. Ukawa for valuable discussions. This work is supported in part by the Grant-in-Aid of the Ministry of Education (No. 04NP0601). Y.K. is supported by a Grant-in-Aid for JSPS fellow.

References

- [1] H.B. Nielsen and M. Ninomiya, Nucl. Phys. **B 185** (1981) 20; Nucl. Phys. **B 193** (1981) 173 .
- [2] L.H. Karsten, Phys. Lett. **B 104** (1981) 315.
- [3] P.D.V. Swift, Phys. Lett. **B 145** (1984) 256.
- [4] J. Smit, Acta Phys. Polon. **B17** (1986) 531.
- [5] S. Aoki, Phys. Rev. Lett. **60** (1988) 2109; Phys. Rev. **D 38** (1988) 618.

- [6] K. Funakubo and T. Kashiwa, Phys. Rev. Lett. **60** (1988) 2113; Phys. Rev. **D 38** (1988) 2602.
- [7] W. Bock, A.K. De, K. Jansen, J. Jersák, T. Neuhaus and J. Smit, Phys. Lett. **B 232** (1989) 486; Nucl. Phys. **B 344** (1990) 207.
- [8] S. Aoki, I-H. Lee, J. Shigemitsu and R. Shrock, Phys. Lett. **B 243** (1990) 403.
- [9] W. Bock and A.K. De, Phys. Lett. **B 245** (1990) 207.
- [10] J. Smit, Nucl. Phys. **B** (Proc. Suppl.) **9** (1989) 579.
- [11] S. Aoki, I-H. Lee and S.-S. Xue, BNL Report 42494(1989); Phys. Lett. **B 229** (1989) 79; I-H. Lee, Nucl. Phys. **B** (Proc. Suppl.) **17** (1990) 457.
- [12] S. Aoki, I-H. Lee, and R.E. Shrock, Nucl. Phys. **B 355** (1991) 383; Nucl. Phys. **B** (Proc. Suppl.) **20** (1991) 589.
- [13] M.F.L. Golterman and D.N. Petcher, Phys. Lett. **B 247** (1990) 370.
- [14] W. Bock, A.K. De and J. Smit, Nucl. Phys. **B 388** (1992) 243.
- [15] M.F.L. Golterman, D.N. Petcher, and E. Rivas, Nucl. Phys. **B 377** (1992) 405
- [16] M.F.L. Golterman and D.N. Petcher, Phys. Lett. **B 225** (1990) 159.
- [17] P. Hasenfratz and H. Leutwyler, Nucl. Phys. **B 343** (1990) 241.
- [18] U. Wolff, Phys. Rev. Lett. **62** (1989) 361.
- [19] M. Lüscher and P. Weisz, Nucl. Phys. **B 300**[FS22] (1988) 325; Phys. Lett. **B 212** (1988) 325.
- [20] T.Nakagawa and Y.Oyanagi, “Program system SALS for Nonlinear Least Squares Fitting in Experimental sciences” in Recent Development in Statistical Inference and Data Analysis, K.Matusita, editor,p. 221–225 (North Holland Publishing Company, Amsterdam, 1980)

Table captions

Table 1. Simulation parameters for scalar fields. The symbol K represents 1,000 configurations.

Table 2. Simulation parameters for fermions. Metro. means Metropolis algorithm. Separation means the number of Monte Carlo sweeps between configurations.

Table 3. Parameter E_ϕ and wave function renormalization constant Z_ϕ for scalar fields and the value of v and z^2 .

Table 4. Fermion masses in the broken phase on an $8^3 \times 16$ lattice. The minimum value of t for fit is denoted by t_{min} .

Table 5. Numerical value of the scalar field propagator $D_g(t)$ in the symmetric phase at $\kappa = 0.145$ on an $8^3 \times 16$ lattice.

Table 6. Neutral fermion mass in the symmetric phase.

Figure captions

Figure 1. σ propagator $D_\sigma(t)$ in the broken phase on an $8^3 \times 16$ lattice. The solid line represents the fit.

Figure 2. Same as Fig.1 for the π propagator $D_\pi(t)$.

Figure 3. Fermion masses as a function of y in the broken phase on an $8^3 \times 16$ lattice. Open circles (filled circles) represent the neutral fermion (neutral doubler) mass and open squares represent the charged fermion mass. The dotted line represents the prediction of the hopping parameter expansion (HPE) for the neutral fermion mass.

Figure 4. Propagator $D_g(t)$ for the scalar field g in the symmetric phase on an $8^3 \times 16$ lattice (filled circle) and a $12^3 \times 16$ lattice (open squares). The solid line represents the fit for the data on a $8^3 \times 16$ lattice.

Figure 5. Neutral fermion propagator $S_N^L(t)$ at $y = 0.4$ (filled circles) and $y = 0.1$ (open circles) in the symmetric phase on an $8^3 \times 16$ lattice. Dotted lines represent the prediction of the hopping parameter expansion (HPE) for neutral fermion propagators.

Figure 6. Neutral fermion masses as a function of y in the symmetric phase on an $8^3 \times 16$ lattice (filled circles) and a $12^3 \times 16$ lattice (open squares). Dotted line represents the prediction of the hopping parameter expansion (HPE) for the neutral fermion mass.

Figure 7. Charged fermion propagator $S_C^L(t)$ at $y = 0.4$ in the symmetric phase on an $8^3 \times 16$ lattice (open circles) and a $12^3 \times 16$ lattice (open squares). Vertical bars connected by solid (dotted) lines represent the data of ref.[14] for the same parameters on an $8^3 \times 16$ (a $12^3 \times 16$) lattice.

Figure 8. Fitted value of E_C as a function of t_{min} in the symmetric phase at $y = 0.4$ on an $8^3 \times 16$ lattice (open circle) and $12^3 \times 16$ lattice (filled circle).

Figure 9. Charged fermion propagator $S_C^L(t)$ at $y = 0.4$ in the symmetric phase on an $8^3 \times 16$ lattice (filled circle) and $12^3 \times 16$ lattice (open

circle), together with the prediction of the large w expansion including the next-to-leading order (solid lines). Dotted lines represent the convolution of $S_N^L(t)$ and $D_g(t)$, which is the leading order contribution in the expansion.

Figure 10. Same as Fig.9 at $y = 0.1$.

Figure 11. Charged fermion propagators $S_C^R(t)$ at $y = 0.4$ in the symmetric phase on an $8^3 \times 16$ lattice (filled circle) and a $12^3 \times 16$ lattice (open circle), together with the prediction by the large w expansion (solid lines).

Figure 12. Same as Fig.11 for $S_C^M(t)$.

Figure 13. Charged fermion propagators, $S_C^L(t)$, at $y = 0.3$ in the broken phase. The meaning of symbols are the same as the Fig.9.

Table 1:

	Broken		Symmetric		
κ	0.16		0.145		
size	$8^3 \times 16$		$8^3 \times 16$	$12^3 \times 16$	
algorithm	Metropolis	Cluster	Metropolis	Cluster	Metropolis
#sweeps	80K	80K	1,200K	240K	900K
#bin	4	8	12	24	18
bin size	20K	10K	100K	10K	50K

Table 2:

	Broken		Symmetric			
κ	0.16 (Metro.)		0.145(Metro.)			
size	$8^3 \times 16$		$8^3 \times 16$		$12^3 \times 16$	
fermion	neutral	charged	neutral	charged	neutral	charged
y	0.1,0.2,0.3		0.1/0.4	0.1,0.4	0.4	
separation	200		500		250	
# conf.	400		600/2,400	2,400	800	3,600
# bin	4		3 / 12	12	4	18
bin size	100		200		200	
source	point		wall			

Table 3:

κ	0.16		0.145		
size	$8^3 \times 16$		$8^3 \times 16$		$12^3 \times 16$
algorithm	Metro.	Cluster	Metro.	Cluster	Metro.
E_σ	0.809(3)	0.813(30)	0.415(2)	0.419(4)	0.412(2)
Z_σ	2.78(15)	2.76(18)	3.36(13)	3.33(19)	3.37(13)
E_π	0	0	0.416(3)	0.409(4)	0.410(2)
Z_π	5.94(5)	5.87(8)	3.39(17)	3.34(24)	3.37(12)
E_g	—	—	0.415(1)	0.414(3)	0.411(2)
Z_g	—	—	6.73(13)	6.66(23)	6.75(15)
v	0.401(1)	0.402(1)	—	—	—
z^2	0.303(1)	0.304(1)	0.177(1)	0.177(4)	0.176(1)

Table 4:

y	$t_{min.}$	0.1	0.2	0.3
E_N^-	0	0.15(1)	0.277(7)	0.384(7)
E_N^+	0	1.7(2)	1.76(9)	1.71(8)
E_{ND}	6	1.4(3)	1.3(2)	1.5(2)
E_C	3	0.149(24)	0.277(1)	0.386(16)
	4	0.152(49)	0.276(11)	0.38(2)
	5	0.168(83)	0.283(19)	0.38(7)

Table 5:

t	D_g	S_C^L	
	$8^3 \times 16$	$8^3 \times 16$	$12^3 \times 16$
0	7.905(9)	0.083(98) ($\times 10^{-4}$)	0.048(49) ($\times 10^{-4}$)
1	5.227(9)	0.1694(1)	158.6(3)
2	3.466(1)	41.7(4)	33.1(3)
3	2.31(1)	13.6(5)	9.3(2)
4	1.55(1)	4.8(3)	2.6(7)
5	1.07(1)	2.2(1)	0.88(5)
6	7.75(1)	0.90(1)	0.33(3)
7	6.16(1)	0.49(6)	0.15(2)
8	5.66(2)	0.36(8)	0.12(1)
9	6.16(1)	0.47(9)	0.17(2)
10	7.75(1)	0.85(1)	0.35(3)
11	1.07(1)	1.9(1)	0.87(5)
12	1.55(1)	4.8(3)	2.8(1)
13	2.31(1)	13.1(5)	9.3(2)
14	3.466(1)	40.2(6)	33.1(3)
15	5.227(9)	168.8(1)	159.9(5)

Table 6:

size		$y = 0.1$	0.4
$8^3 \times 16$	E_N^-	0.1895(1)	0.5491(6)
	E_N^+	1.109(1)	1.458(2)
$12^3 \times 16$	E_N^-	—	0.5495(1)
	E_N^+	—	1.4562(9)

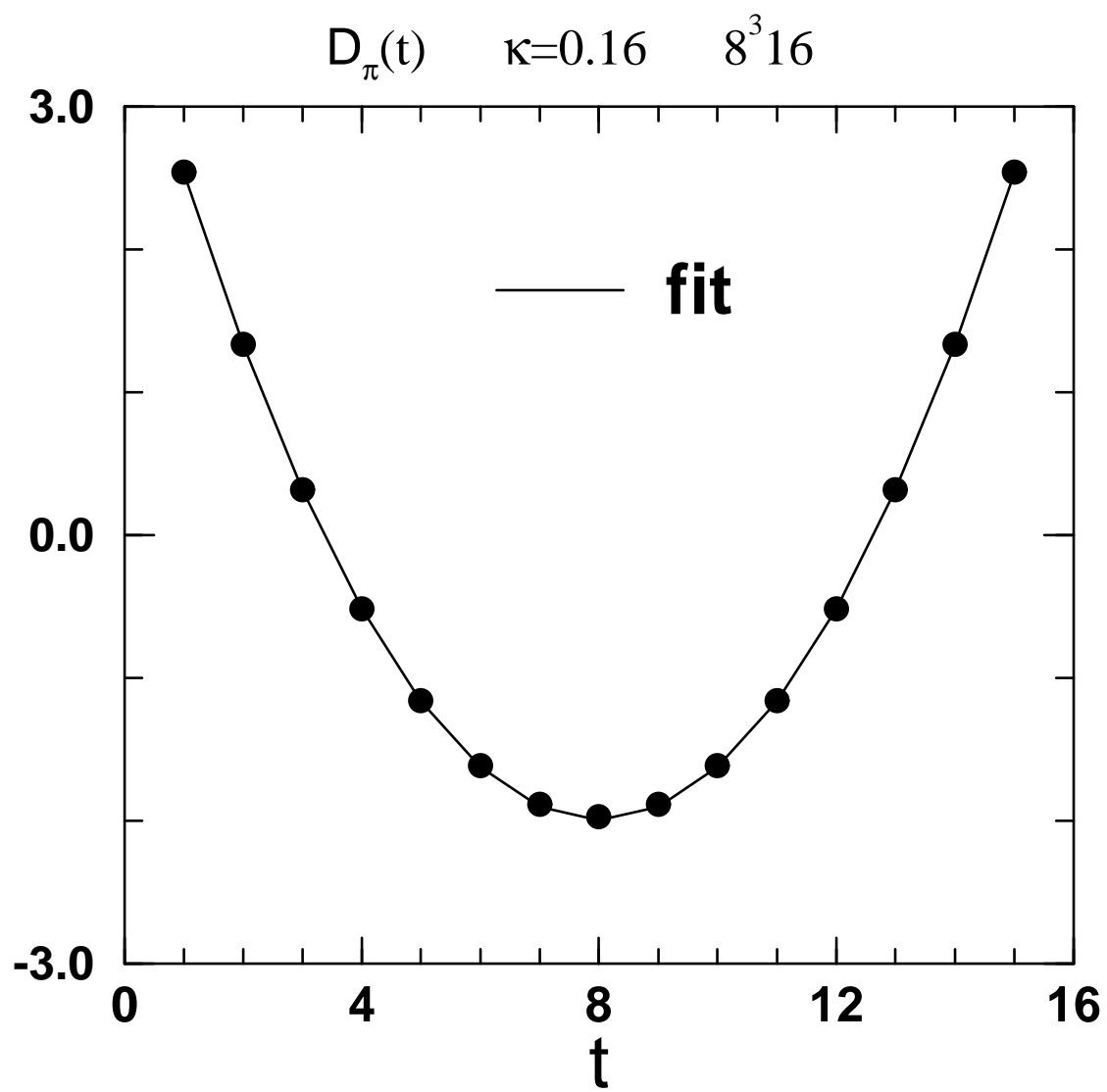


Figure 1:

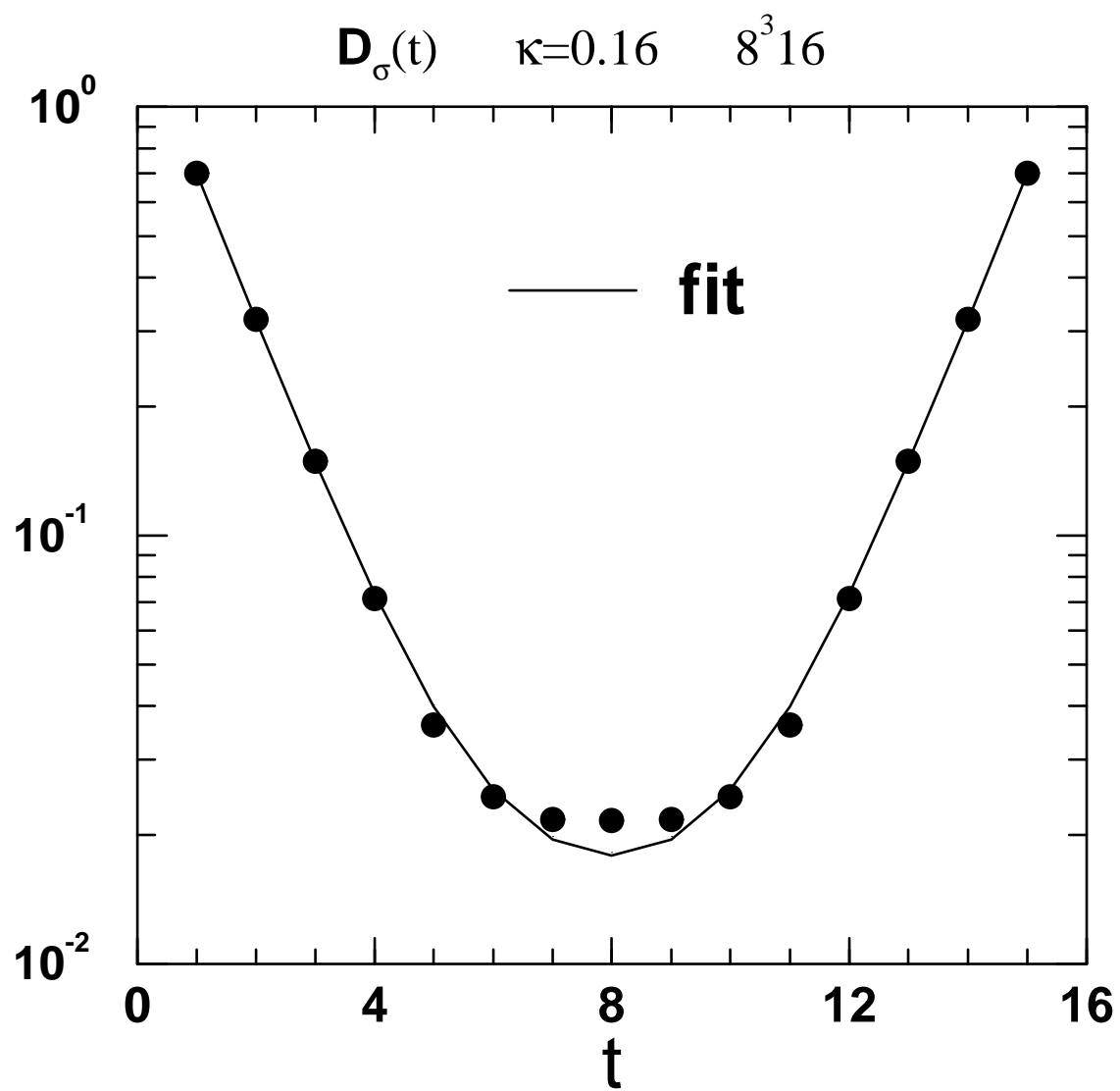


Figure 2:

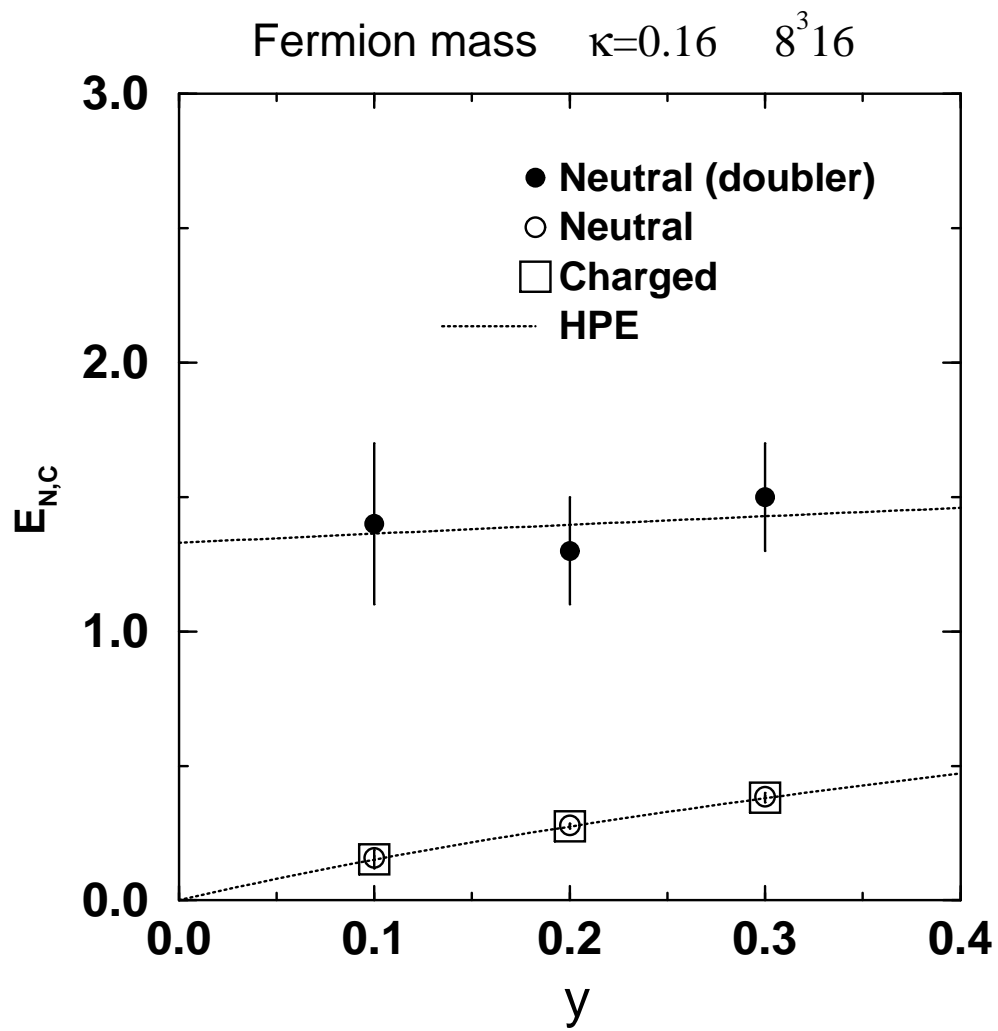


Figure 3:

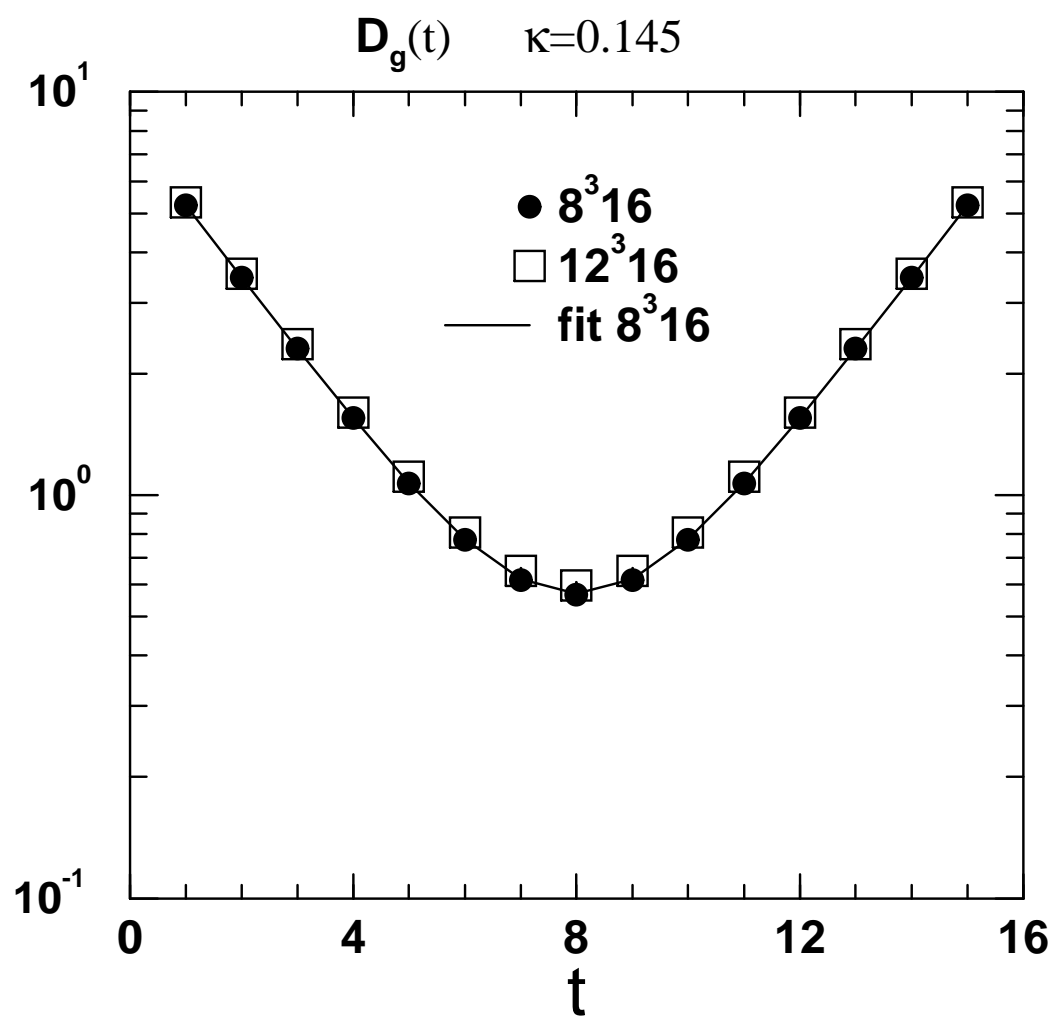


Figure 4:

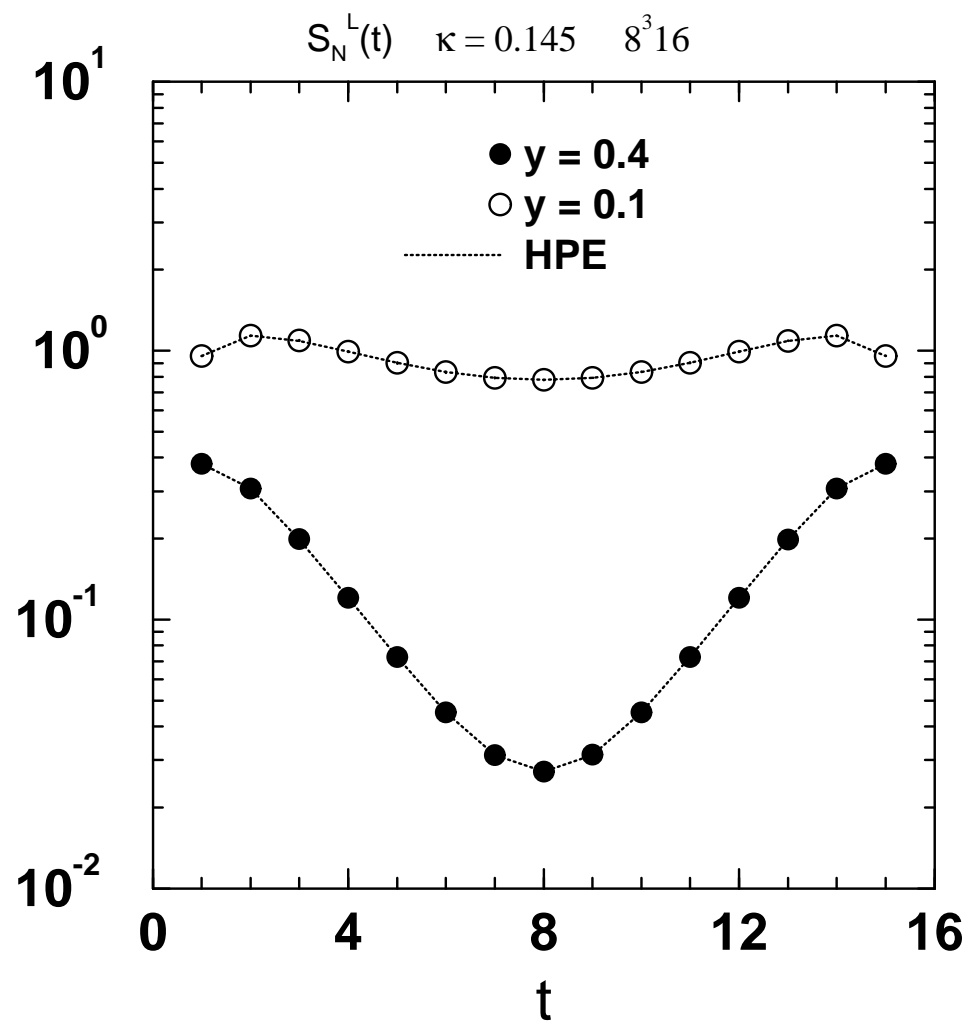


Figure 5:

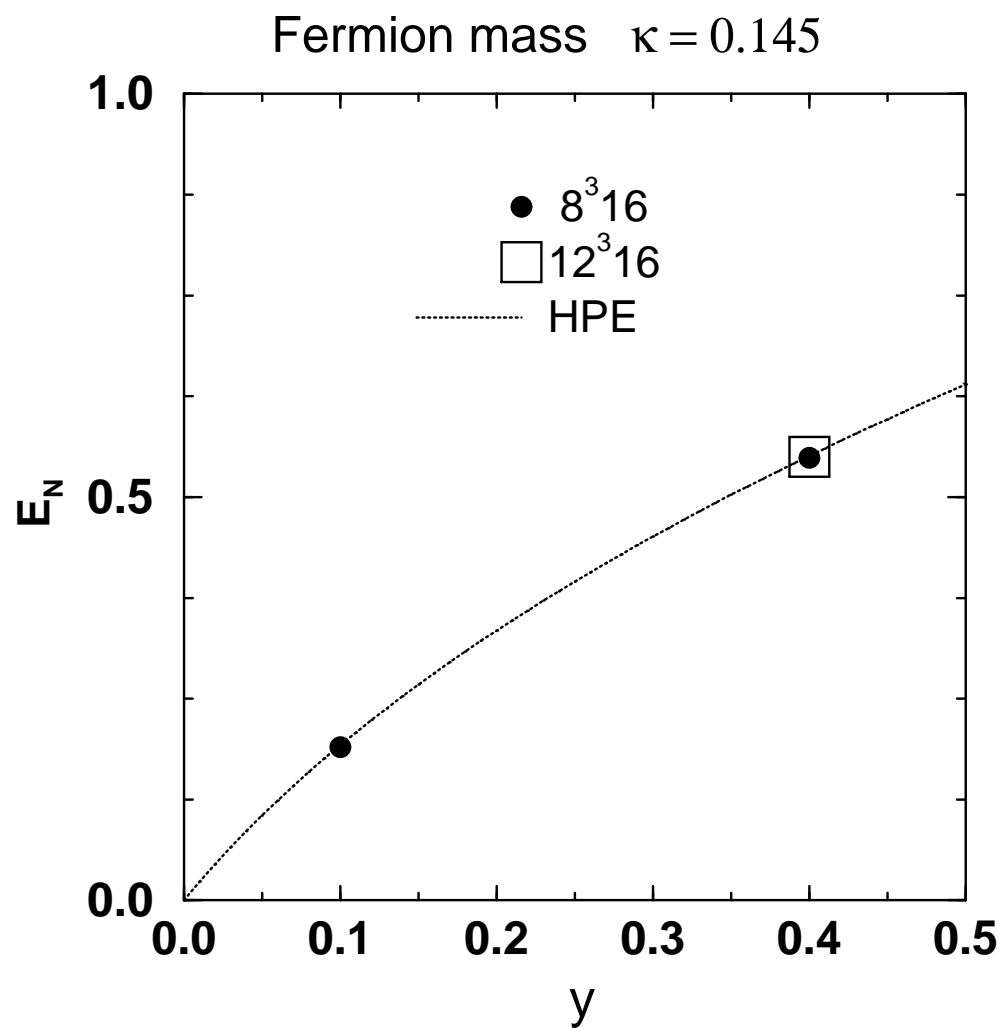


Figure 6:

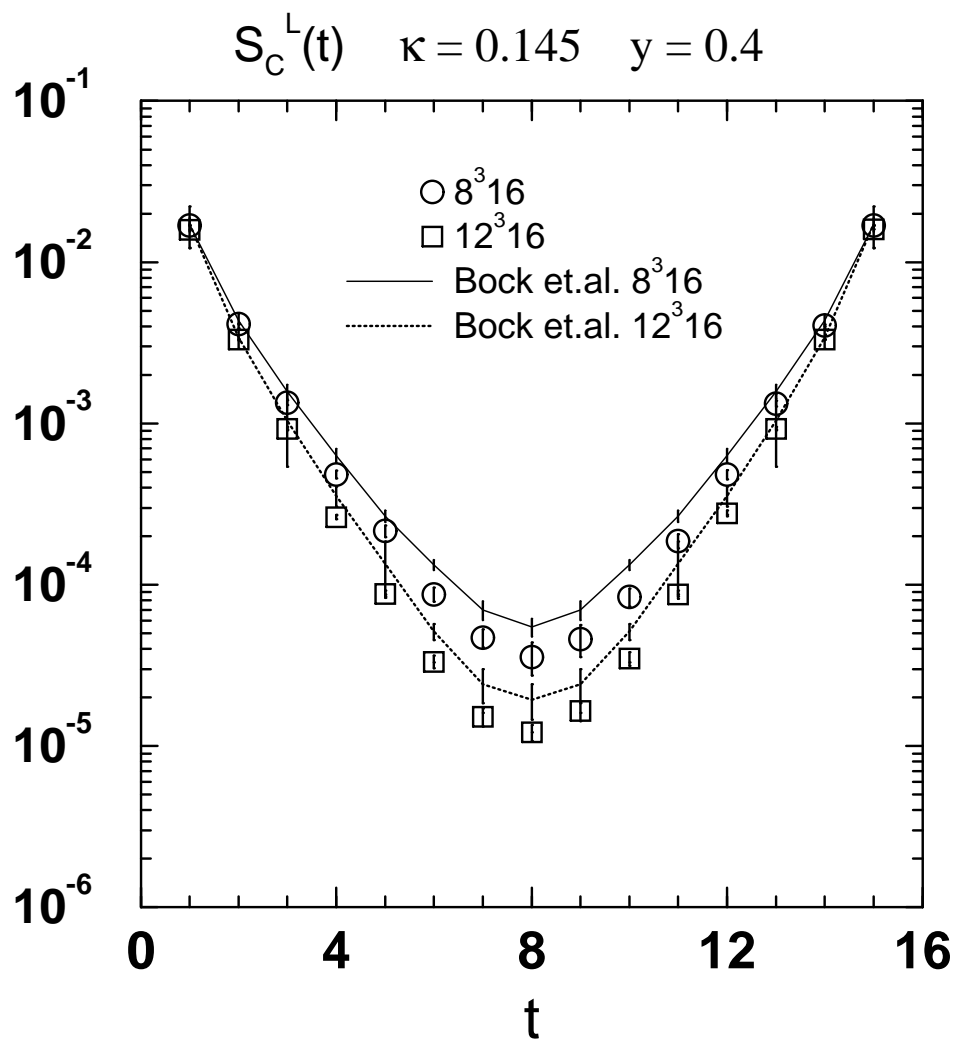


Figure 7:

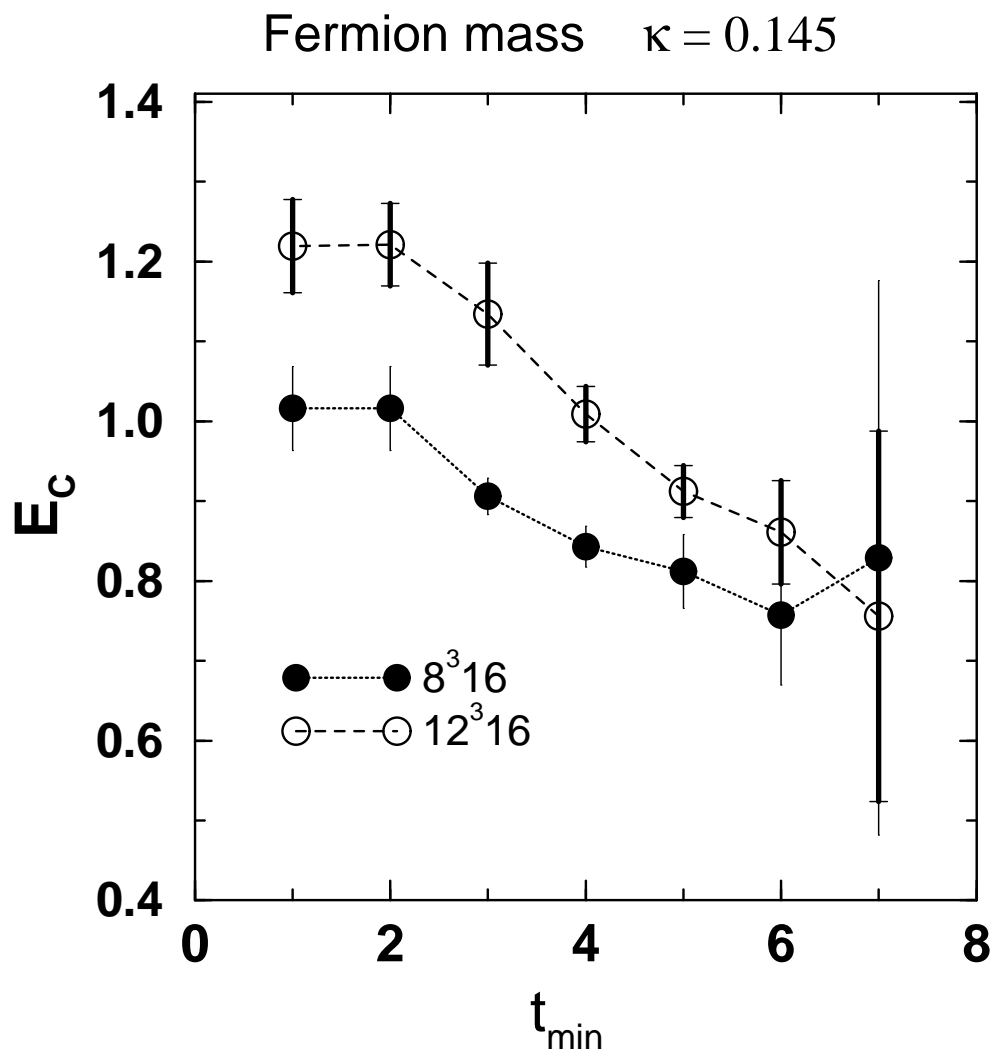


Figure 8:

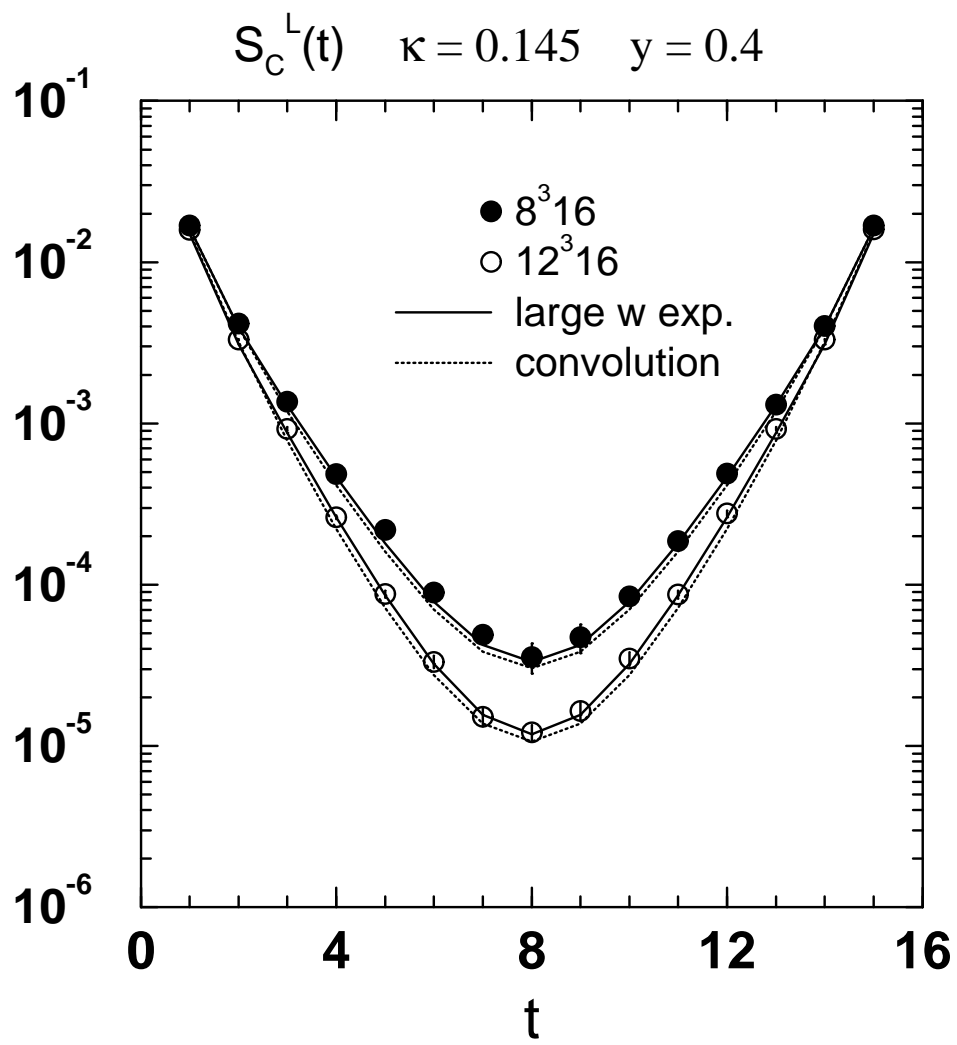


Figure 9:

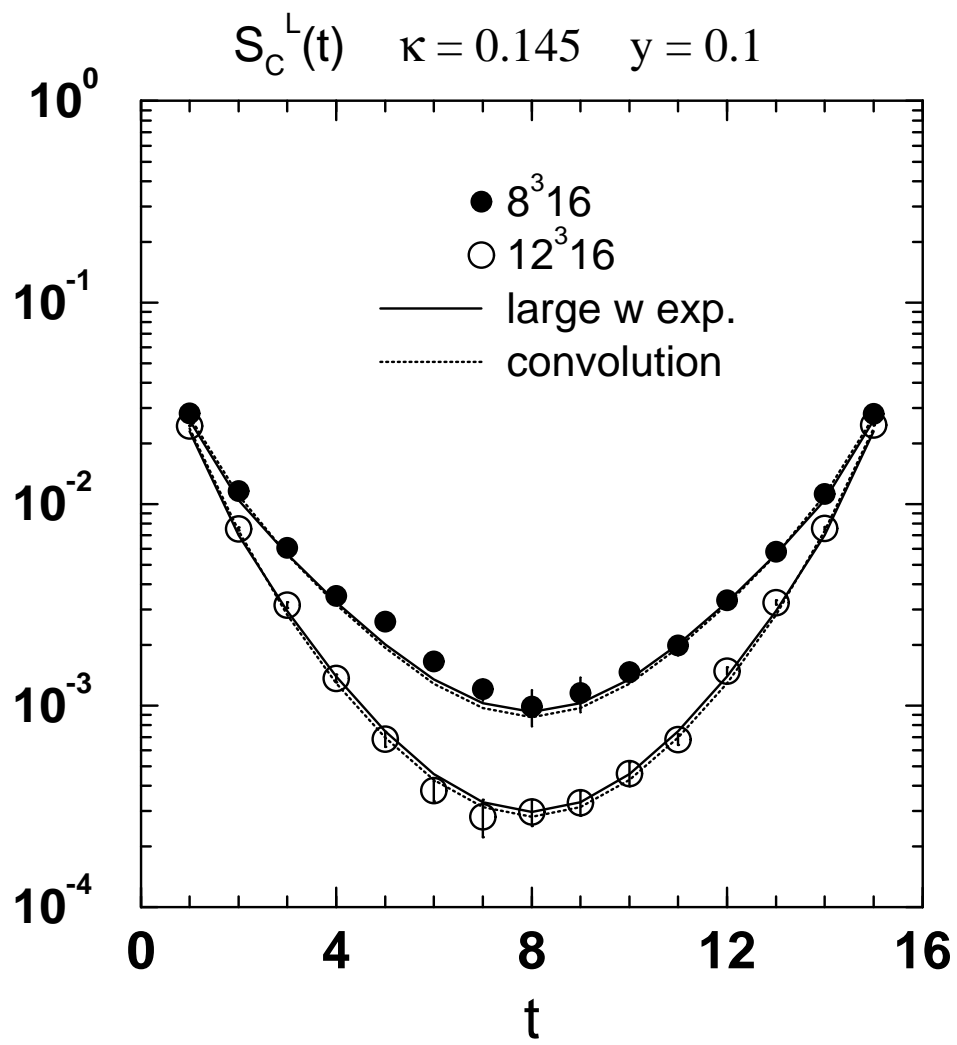


Figure 10:

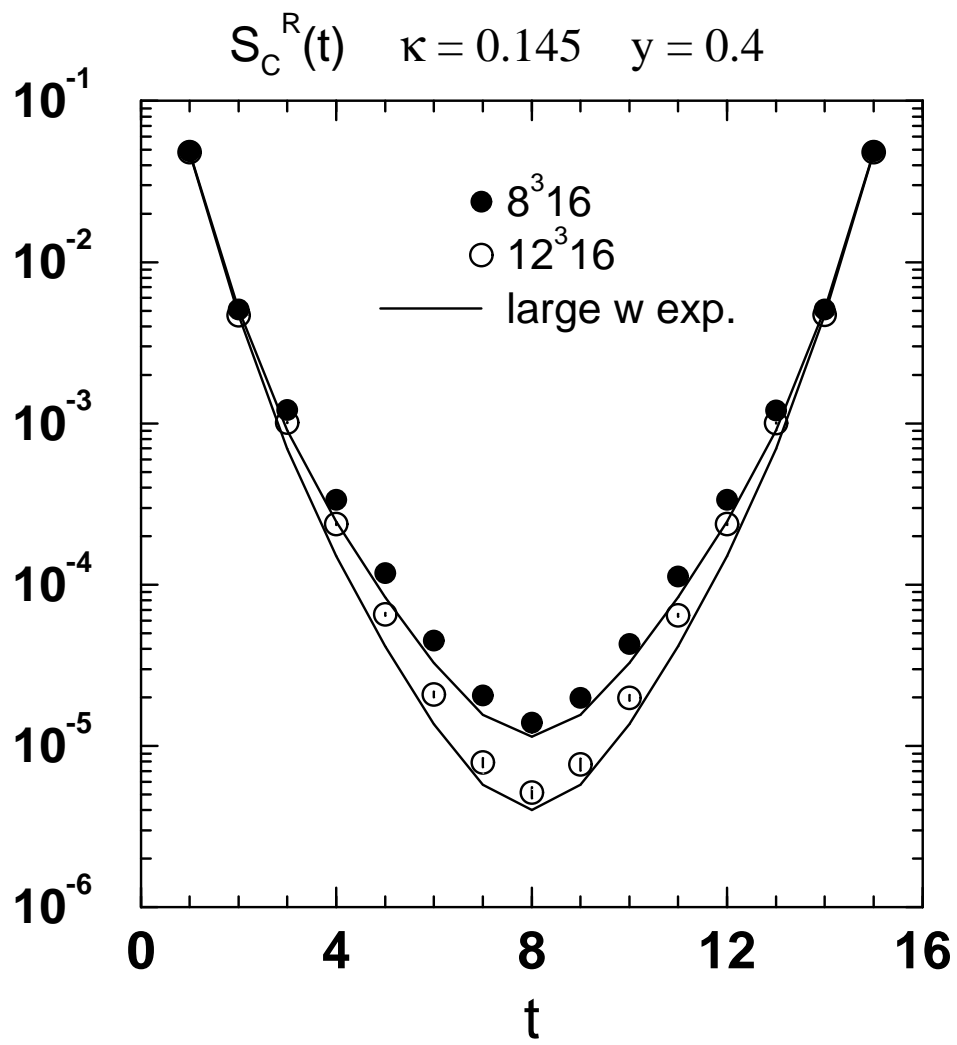


Figure 11:

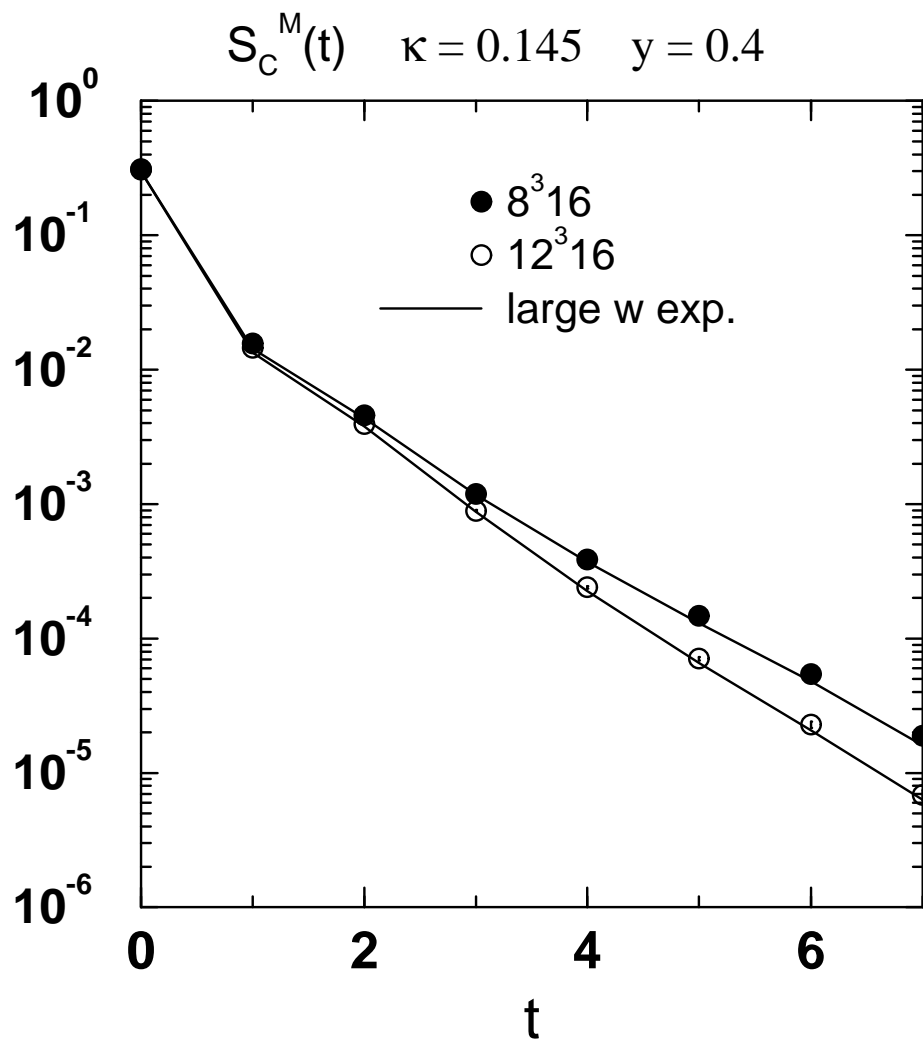


Figure 12:

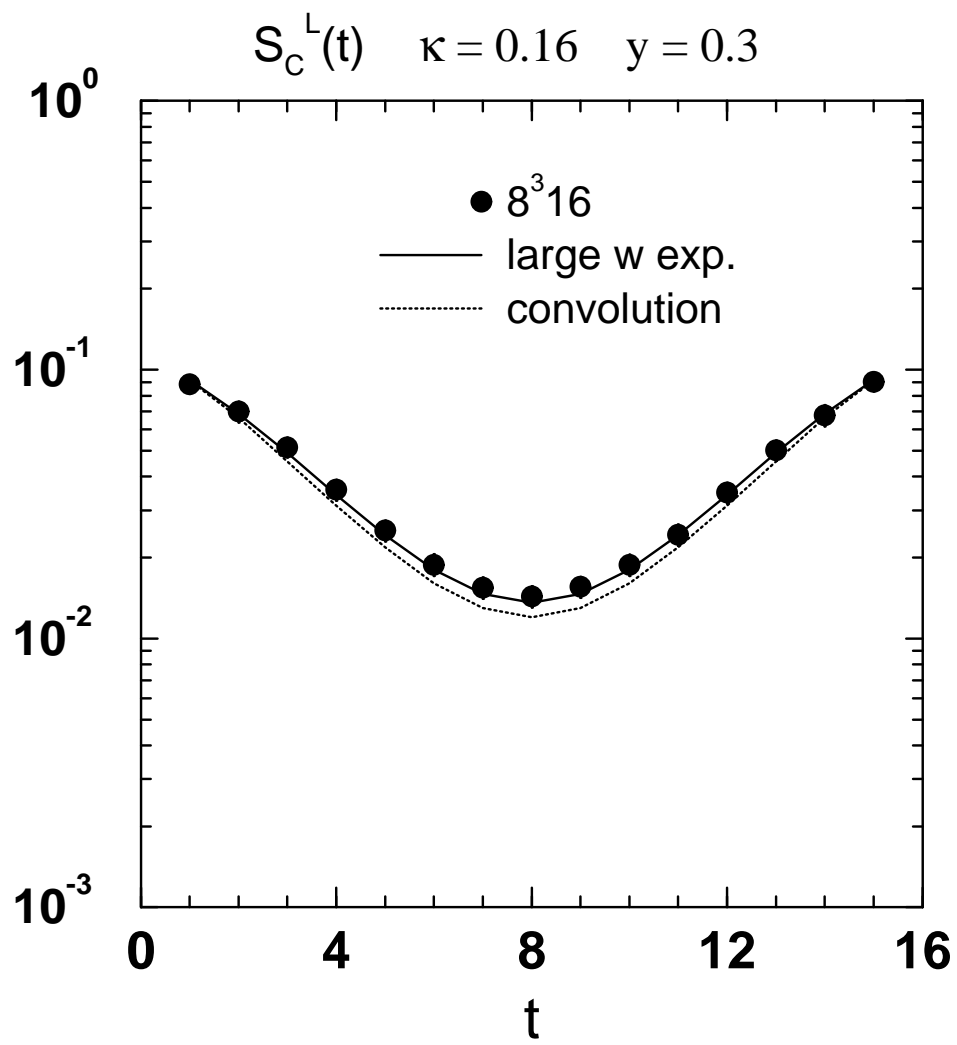


Figure 13: